1   **Surface Albedo Darkening from Wildfires in Northern Sub-Saharan Africa**

2   C. K. Gatebe[a,b], C.M. Ichoku,[a] R. Poudyal,[a,c] M.O. Román,[a] and E. Wilcox, [d]

3   *[a]NASA Goddard Space Flight Center, Greenbelt, Maryland, 20771, USA.*

4   *[b]Universities Space Research Association, Columbia, Maryland, 21228, USA.*

5   *[c]Science Systems and Applications, Inc., Lanham, Maryland, USA.*

6   *[d]Desert Research Institute, Reno, Nevada, 89512, USA.*

7   *Correspondence: Charles Gatebe: charles.k.gatebe@nasa.gov*

8   **Abstract**: Wildfires are recognized as a key physical disturbance of terrestrial ecosystems and a

9   major source of atmospheric trace gases and aerosols. They are known to produce changes in land-

10   scape patterns and lead to changes in surface albedo that can persist for long periods. Here, we es-

11   timate the darkening of surface albedo due to wildfires in different land cover ecosystems in North-

12   ern Sub-Saharan Africa using data from the Moderate Resolution Imaging Spectroradiometer

13   (MODIS). We determined a decrease in albedo after fires over most land cover types (e.g. woody

14   savannas: (-0.00352 ± 0.00003) and savannas: (-0.00391±0.00003), which together accounted for

15   >86% of the total MODIS fire count between 2003 and 2011). Grasslands experienced a larger de-

16   crease (-0.00454± 0.00003) than the savannas, but accounted for only about 5% of the total fire

17   count. A few other land cover types (e.g. Deciduous broad leaf: (0.00062 ± 0.00015), and barren:

18   (0.00027 ± 0.00019)), showed an increase in albedo after fires, but accounted for less than 1% of

19   the total fires. Albedo change due to wildfires is more important during the fire season (October-

20   February). The albedo recovery progresses rapidly during the first year after fires, where savannas

21   show the greatest recovery (>77%) within one year, while deciduous broadleaf, permanent wetlands

22   and barren lands show the least one-year recovery (56%). The persistence of surface albedo darken-

23   ing in most land cover types is limited to about six to seven years, after which at least 98% of the

24   burnt pixels recover to their pre-fire albedo. The albedo recovery after fires can be described by a

25   simple exponential function.

26

26 **1.   Introduction**

27   Wildfires are recognized as a key physical disturbance of terrestrial ecosystems and

28 a significant source of atmospheric trace gases and aerosols (e.g. Roberts et al., 2009; An-

29 dreae & Merlet, 2001; Bremer et al., 2004). Since biomass burning depends primarily on

30 fuel availability that is controlled by mean annual precipitation and soil fertility (Gita et al.,

31 2012), intense fire activities are normally observed when vegetation is dry (Eva & Lambin,

32 1998). In Africa, most intense biomass burning is observed in the northern sub-Saharan

33 Africa between December and February, and in southern Africa between July and Novem-

34 ber (Scholes & Archer, 1997). These fires are believed to have shaped the savannas vegeta-

35 tion more than any other disturbance (Sheuyange et al., 2005). So there is a strong linkage

36 between biomass burning, weather and climate (cf. Randerson et al., 2006; Dale et al.,

37 2001; Crutzen and Andreae, 1990).

38   The extent of wildfires in Africa can be seen clearly from a map of active fire de-

39 tected by satellite sensors such as the Moderate Resolution Imaging Spectroradiometer

40 (MODIS) at their times of overpass under relatively cloud-free conditions. In the northern

41 Sub-Saharan Africa (NSSA) region, most fires are detected south of the Sahara desert al-

42 most across the whole region from west to east (Fig. 1a). Some areas such as Southern

43 Sudan appear to be more fire-prone than others, as nearly every square km of land seems to

44 have been affected by fire at least once between 2003 and 2011 (cf. Figure 1a: inset). Dur-

45 ing that nine-year period, with approximately two overpasses by Terra every 24 hours (once

46 during the day and once at night), the total MODIS active fire-pixel count at 1-km resolu-

47 tion in the entire NSSA region is about 2.2 million, with an annual average of about 11% of

48 the total fire count. Indeed, Africa has the highest frequency of occurrence of fire per land

49 area than any other continent (Ichoku et al., 2008). These fire statistics are likely an under-

50 estimate of the actual fire activity, since smaller and cooler fires are probably missed due to

51   the relatively high thresholds used in the MODIS global fire detection algorithm (Giglio et

52   al., 2003; Justice et al., 2002). Some of the factors that can influence fire detection by satel-

53   lite sensors such as MODIS relate to their orbital and viewing geometry, fire growth rates,

54   fire intensity and size, and fire obscuration by clouds, smoke and atmospheric moisture

55   (Eva & Lambin, 1998). The occurrence of wildfires is more frequent in the savannas

56   (woody savannas and savannas), and account for >86% of the total MODIS fire count be-

57   tween 2003 and 2011 (discussed later in section 3.1; c.f. Table 4, column 2; Fig. 1b).

58   Hence, the spatial-temporal extent of vegetation fires in sub-Saharan Africa is widespread,

59   and the disturbance rates from year to year remain uniform based on MODIS fire count be-

60   tween 2003 and 2011. The effects of wildfires can extend beyond the vegetation it con-

61   sumes, but the processes that couple the effects of fires on the surface and ecosystems to

62   regional climate (through albedo and water/energy flux) and to global climate (through

63   CO_2 and CH_4) remain uncertain. This indicates a need to improve our understanding of

64   vegetation fires in Africa, which represents the largest fire region in the world.

65   There are many possible effects from fires that have been found to manifest through

66   changes in albedo, or the energy exchange between land and the atmosphere (e.g. Govaerts

67   et al., 2002; O'Halloran et al. 2012; Jin & Roy, 2012; Chapin et al. 2000; Chambers et al.

68   2005), evapotranspiration (Bosch & Hewlett, 1982; Zhang et al., 2001), rainfall interception

69   (Levia & Frost, 2003), runoff (Farley et al., 2005), and streamflow (Jackson et al., 2005).

70   Therefore, fires can cause multiple effects that operate through changes in albedo, rough-

71   ness length, and water transport properties from soil to the atmosphere, including leaf area

72   index, stomatal conductance, and rooting depth. Other effects include changes in the carbon

73   mass balance in terrestrial ecosystems, as well as the production of carbonaceous aerosols

74   and trace gases (Randerson et al., 2006). Fires also change the cycling of carbon and nutri-

75   ents between soil, vegetation and the atmosphere during the burning of woody debris such a

76   fallen twigs, dead grass and leaf litter (Andersen et al., 2003). In the case of radiative for-

77   cing, wildfires can significantly alter surface albedo and create a positive radiative forcing

78   by increasing the amount of solar radiation absorbed in the climate system, especially over

79   the boreal forests (O'Hallon et al., 2012; Randerson et al., 2006). However, this albedo de-

80   pendence is difficult to quantify properly owing to a large spatial and temporal variability

81   as a result of other factors such as seasonal changes in vegetation cover, rainfall, and inten-

82   sification of land use as measured by population density (Fuller and Ottke, 2002).

83   This study focuses on changes in surface albedo associated with biomass burning in

84   the NSSA region, which is less studied compared to other areas such the boreal forests and

85   subarctic sites (Amiro et al. 1999; 2006). Fires are believed to be a major driver of the car-

86   bon, energy, and water cycles in the NSSA due to their enormous heat release, and an

87   abundance of gaseous and particulate smoke emissions. The NSSA region comprises a

88   wide range of vegetation and climatic zones over a relatively small latitudinal belt from 5–

89   20°N (Fig. 1b), and has become a focal point of debates over desertification, deforestation,

90   and climate change (Fuller and Otke, 2002). This study is a part of an interdisciplinary ef-

91   fort investigating the effects of intense biomass burning on the declining regional water re-

92   sources as exemplified by the drying of Lake Chad (Le Houérou, 1996). The interdiscipli-

93   nary study seeks to assess surface, atmospheric and water cycle processes in the region

94   through remote sensing and modelling approaches that integrate research, systems engi-

95   neering, and applications expertise to best make the connections between various identified

96   processes and phenomena. Such an approach ensures concrete results for societal benefits

97   and climate assessments.

98   The results of the albedo analysis presented in this paper are expected to provide

99   critical input to various models used in the different aspects of the broader interdisciplinary

100 research. They will be used in the land-surface models to determine the effects of albedo

101 changes due to fires on soil moisture budget, evapotranspiration, infiltration, and runoff, all

102 of which govern the land-surface component of the water cycle. Also, our surface albedo

103 change results will be ingested in atmospheric models, where they will serve as part of the

104 essential input parameters based upon which radiative energy budget estimates are made,

105 both at the surface and at the top of the atmosphere (TOA). As such, these models can bet-

106 ter characterize the effects of change in surface albedo due to fires on the atmospheric heat-

107 ing rates of the black carbon (BC) aerosols emitted by fires, which can affect the atmos-

108 pheric component of the water cycle through the interaction of radiation with surface al-

109 bedo and the aerosol indirect radiative effects on clouds. Furthermore, information on the

110 spatial and temporal dynamics of the post-fire albedo recovery will be important in model-

111 ling the medium- to long-term climate impacts of fires in the NSSA region.

112 The remainder of this paper is organized into three main sections. Section 2, data and

113 methods, describes the MODIS albedo data, albedo gap filling, and determination of albedo

114 change and recovery. Section 3 presents our results of the albedo change and recovery fol-

115 lowing fire activities for different land cover types in the NSSA region. Section 4 concludes

116 with a summary of the study.

117 **2. Data and Methods**

118 *2.1 MODIS Albedo*

119 Satellites are ideal for providing observations needed for description of surface al-

120 bedo on a global scale, but we must contend with issues such as uncertainty of the meas-

121 urements due to atmospheric effects, inadequate sampling (spectral, spatial and temporal),

122 and directionality of these measurements. The global MODIS (Collection 5) albedo pro-

123 duct, MCD43A3, (https://lpdaac.usgs.gov/products/modis_products_table/, 1 September

124   2012) combines measurements from both Terra and Aqua satellites to retrieve directional

125   hemispherical reflectance (black-sky albedo) and bihemispherical reflectance (white-sky

126   albedo) at local solar noon as both spectral (seven narrow spectral bands, MODIS channels

127   1–7; http://modis.gsfc.nasa.gov/about/specifications.php, 1 September 2012) and three

128   broadband (0.3–0.7 µm, 0.7–5.0 µm, and 0.3–5.0 µm) quantities.

129   The albedo is derived from the BRDF (bidirectional reflectance-distribution func-

130   tion) model parameters that are retrieved from all high-quality, cloud-free, atmospherically

131   corrected surface reflectance, acquired sequentially over a 16-day period at a spatial resolu-

132   tion of 500 m. The 16-day interval provides an appropriate trade-off between the availab-

133   ility of sufficient angular samples and the temporal stability of the surface (Schaaf et al.,

134   2002; Wanner et al., 1997). However, the assumption of stability becomes more tenuous

135   during periods of strong phenological change such as vegetation green-up, senescence, har-

136   vesting, or even snowfall or meltdown, when surface characteristics change abruptly. The

137   synergistic use of MODIS observations from both Terra and Aqua offers an opportunity to

138   increase the angular sampling, and helps to improve the coverage and quality of global

139   BRDF and albedo retrievals (Salomon et al., 2006). Note that Terra has a descending equa-

140   torial crossing time of 10:30 a.m., while Aqua has an ascending orbit with a 1:30 p.m.

141   equatorial crossing time. High quality retrievals are obtained during periods of intermittent

142   clear-sky observations by overlapping processing of the data such that retrievals are at-

143   tempted every eight days (based on all clear sky observations over the 16 days). However,

144   during long periods of clear sky conditions, the 8-day overlapping introduces an autocorre-

145   lation between retrievals, since some of the observations wind up being used in more than

146   one period of retrieval (Schaaf et al., 2002).

147   We used high-quality white-sky broadband albedo (0.3–5.0 µm), whose quality is

148   defined by the BRDF and albedo quality product (MCD43A2), to assess the impact of bio-

149   mass burning on surface albedo. The white-sky albedo is derived from BRDF measure-

150   ments, integrated over both incoming and outgoing hemispheres, and does not depend on

151   the illumination and atmospheric conditions. Oftentimes, the high quality retrievals contain

152   significant data gaps (Gao et al. 2008), especially in periods of significant cloud cover,

153   where insufficient angular sampling leads to a magnitude inversion rather than a full-model

154   inversion (Schaaf et al., 2002). A full model inversion is attempted only when at least seven

155   cloud-free observations of the surface are available during a 16-day period, and the direc-

156   tional observations adequately sample the view/illumination geometry.

157   *2.2   Gap Filling Method and Validation*

158   As described in Section 2.1, MODIS albedo time series contains data gaps where

159   albedo is not retrieved because of problems such as low data quality, persistent or cloud

160   contamination, and poor illumination conditions, which lead to insufficient angular sam-

161   pling and a lower accuracy on BRDF and albedo. To address the resulting data gap prob-

162   lem, we developed a simpler algorithm for producing temporally smoothed and spatially

163   complete MODIS white-sky albedo data set. The new gap-filling algorithm first examines

164   each pixel time-series for data gaps and then assigns it one of the five categories deter-

165   mined by the number of consecutive data gaps k in the time-series (k= 1, or 2, or 3, or 4, or

166   ≥4 gaps). Note that the largest data gap (four consecutive missing observations) represents

167   a temporal gap of about a month and the albedo is assumed to be stable or changes slowly

168   except during the transition period. For classes with gaps k =1,…, 4, the missing values are

169   determined from Eq. 1:

170         $$\alpha_t = \alpha_{t-1} + (\frac{\alpha_{t+1} - \alpha_{t-1}}{d_{t+1} - d_{t-1}})(d_t - d_{t-1}) \qquad (1)$$

171   where α_t is the missing albedo value on a Julian day, d_t, α_{t-1} is the last existing al-

172   bedo value in the time series, and α_{t+1} the first albedo value in the time series after the gap.

173   While a majority of the missing values are determined from Eq. 1, the method does not

174   work well when there are more than four consecutive missing values in a time series. In this

175   case, an attempt is made to use neighboring pixels to estimate the missing albedo value

176   within a small window defined by 11 × 11 MODIS 500-m pixels around the missing value,

177   and having the same land cover type as defined by the MODIS Land Cover product

178   (MCD12Q1). If there are no pixels of the same land cover type as the missing value in the

179   selected window, the algorithm progressively increases the search-window size to 31 x 31,

180   or 61 x 61, or 121 × 121, while automatically continuing the search until a suitable albedo

181   match is found. If the algorithm finds no pixels within the maximum search distance (121 ×

182   121 MODIS 500-m pixels), the missing value is replaced by a long-term average albedo

183   derived from the 2003-2011 MODIS albedo of each land-cover type in the entire study re-

184   gion. This approach ensures that every gap is filled with an albedo value that has similar

185   characteristics as the missing pixel and impacted by the same weather systems.

186   To verify the efficacy of the new gap filling algorithm to MODIS measurements,

187   we tested the gap filling method by masking a part of the 'good' data, which were randomly

188   selected from different land cover types, and applied the gap filling method on these obser-

189   vations and then determined the accuracy of the gap filling method. Table 1 shows average

190   errors (%; (estimated − good) /good), where absolute values range from 0.02–2.90% (1-

191   gap), 0.02-5.53% (2-gaps), 0.12–12.90% (3-gaps), and 0.02–21.13 % (4-gaps). The errors

192   seem pretty small for barren, grasslands and open shrubland, but increase with gap length

193   for savannas, crop/natural vegetation, and deciduous broadleaf forests. The new gap-filling

194   method performs well, but generally underestimates the albedo values.

195   We also applied the algorithm to MODIS measurements over a different region in

196   the Southern Great Plains (SGP), Central Facility, Oklahoma, USA. The SGP site has co-

197   incident airborne surface reflectance measurements from NASA's Cloud Absorption Radi-

198   ometer (CAR; Gatebe et al., 2003; King et al., 1986) over a period of 32 days, centered

199   around 24 June 2007 (Day-of-the-year, DOY, 175). The airborne data were acquired during

200   the 2007 Cloud and Land Surface Interaction Campaign (CLASIC'07; Román et al. 2011).

201   That period was dominated by cloudy skies and heavy rainfall in the region, resulting in a

202   lot of missing albedo values (Román et al., 2011) that had to be filled to create a good

203   dataset to evaluate the new gap filling method. Thus, we used the coincident retrievals from

204   CAR to conduct first-order evaluation of the gap filled approach (c.f. Table 2; Fig. 2,

205   MODIS albedo2). We also compared our method to the MODIS temporally smoothed and

206   spatially continuous albedo method by Gao et al., (2008) (c.f. Table 2; Fig. 2, MODIS al-

207   bedo1). Note that we used the full expression for all retrievals from aircraft (CAR) and

208   MODIS gap filled approaches (albedo1 and albedo2), as described in Román et al, (2010).

209   Although MODIS albedo values are systematically biased low against aircraft/CAR albedo

210   and tower based albedo by about 15–20%, the two gap-filling methods (albedo1 and al-

211   bedo2) agree to within 4–5% (cf. Table 2), but the new approach is simpler and uses mainly

212   the most recent values on either side of the gap and land cover to fill the missing values. On

213   the other hand, MODIS gap filling approach (Gao et al., 2008) is much more rigorous and

214   normally fit at least 18 months to adequately capture the phenology and bridge a gap. These

215   systematic differences should have little or no impact on the determination of albedo

216   change due to fires.

217   *2.3   Determination of albedo change due to fires*

218   The albedo change caused by biomass burning was determined at the pixel level for

219   each land cover type using the 2003-2011 MODIS albedo data record in the entire NSSA

220   region on a monthly basis. A pixel was considered burned when an active fire was reported

221   in the MODIS Level-3, 8-day daily active fire product (MOD14A2) at the 1 km grid cell

222   and at all the fire detection confidence (low-confidence fire, nominal-confidence fire, or

223   high-confidence fire). The decision to consider fires in all confidence classes was meant to

224   boost the number of burnt pixels for some land cover types (e.g. permanent wetlands and

225   closed shrublands), especially during the non-fire season months. Overall, the low-

226   confidence cases accounted for <5% of all the MODIS fires detected between 2003-2011

227   for most of the land cover types, and therefore, had little influence on the albedo perturba-

228   tion estimates. The study focuses more on the albedo changes during fire season and as-

229   sumes that all 4 x 500 m MODIS albedo pixels burn for each 1km active fire pixel detec-

230   tion. Here, we define the average albedo change $\Delta\overline{\overline{\Omega}}_c$ due to vegetation fires for land cover

231   type c, at the time of fire, as:

232   $$\Delta\overline{\overline{\Omega}}_c = \overline{\Omega}_c - \overline{\Omega}_{c,0} \qquad\qquad\qquad (2)$$

233   where $\overline{\Omega}_{c,0}$ is the pre-fire albedo of a pixel (albedo before a fire is reported, irrespec-

234   tive of pixel's fire history), averaged over many pixels of the same land cover type c (Table

235   3), and $\overline{\Omega}_c$ is the albedo of the burned pixels, 24 days after fire was reported, averaged over

236   many pixels of the same land cover type c. Note that the 24 days were chosen to minimize

237   autocorrelation caused by the 16-day data processing interval for the MODIS albedo pro-

238   duct, which is produced every eight days. Table 4 shows the monthly albedo change de-

239   rived from various major land cover types in the NSSA region, which constitute 99.7% of

240   the land area, and averaged over nine years of MODIS data from 2003-2011. Note that

241   monthly values are defined by the average of the 8-day retrievals that fall in a calendar

242   month. The standard deviation in each case (Table 4) represents a temporal and spatial

243   variability of the albedo change.

244 **3. Influence of biomass burning on albedo**

245 *3.1 Estimation of albedo changes caused by biomass burning*

246 We estimated changes in the albedo after vegetation fires for 11 major land eco-

247 system types in Africa that were derived from the annual MODIS Land Cover product

248 (MOD12Q), Collection 5 (cf. Fig. 1b; Friedl et al., 2010). Barren or sparsely vegetated

249 lands occupy a large area of the northern Sub-Saharan Africa, 25%, followed by woody sa-

250 vannas, 15%, grassland, 15%, savannas, 11%, open shrubland, 11%, evergreen broadleaf,

251 10%, cropland or natural vegetation, 8%, closed shrubland, 2%, cropland, 2%, persistent

252 wetland, 0.6%, deciduous broadleaf and others, ~0.003%. As noted earlier, the occurrence

253 of fires is most frequent in the savannas (woody savannas and savannas), which accounted

254 for over 86% of the total MODIS fire count between 2003-2011 (cf. Table 4, column 2;

255 Fig. 1b). As shown in Figure 3, most fires in the NSSA occur between October and March,

256 with the peak for some cover types around January or November. Barren or desert land

257 cover type has a peak around May, but this may be a false peak given that fire detection

258 over barren or desert is quite a challenge and oftentimes contains more false alarms com-

259 pared to other land cover types (c.f. Giglio et al., 2003).

260 The albedo change caused by fires varies by ecosystem type as depicted in Fig 4,

261 and detailed in Table 4. Each value represents monthly average albedo perturbation due to

262 vegetation fires for different land cover types in sub-Saharan Africa for a period of nine

263 years (2003-2011). The standard deviation accounts for temporal and spatial variability of

264 the albedo perturbation due to fires. Some ecosystems show large values of the standard

265 deviation partly because of post-fire changes in surface albedo associated with dissipation

266 of charcoal and ash, and vegetation regrowth over the 24 days period used to calculate

267 monthly post-fire albedo change (cf. Amiro et al. 2006; Jin & Roy, 2005). Figure 4a shows

268 total albedo perturbation for all months in each land cover type, which show an increase in

269 albedo except in barren and evergreen broadleaf forests. But given that most fires occur be-

270 tween October and February in the NSSA region (cf. Fig. 3), we decided to aggregate al-

271 bedo change values for the fire season months (October-February).

272 Figure 4b shows the albedo change during the biomass burning season, where most

273 land cover types now show a decrease in albedo after fires, except for a few land cover

274 types (e.g. deciduous broadleaf forests). Both evergreen broadleaf forests and grasslands

275 show the highest albedo decrease ((-0.00590 ± 0.00015) and (-0.00454 ± 0.00003), respec-

276 tively), followed by savannas (-0.00352 ± 0.00003), croplands/natural vegetation (-

277 0.00374±0.00002), woody savannas (-0.00352 ± 0.00003), open shrublands (-

278 0.00266±0.00002), and croplands (-0.00110 ± 0.00003). The four land cover types that

279 show an increase after fires are permanent wetlands (0.00340±0.00010), closed shrublands

280 (0.00144 ± 0.00003), deciduous broadleaf forest (0.00062±0.00008), and barren

281 (0.00027±0.00019). The change in albedo associated with fires is more important where

282 most fires are reported (e.g. woody savannas (48.69%), savannas (37.73)%, crop/natural

283 vegetation (5.59%) and grasslands (4.78%)), which together accounted for about 97% of all

284 the MODIS fires detected between 2003 and 2011. Some studies have suggested that the

285 observed differences in albedo change among different land covers are likely related to dif-

286 ferences in fuel composition and combustion characteristics, with generally higher combus-

287 tion completeness observed in grasslands than woodlands (Jin & Roy, 2005; Roy et al.

288 2008; Hoffa et al., 1999). Figure 4c show spatial distribution of albedo perturbation, as-

289 suming that fires would burn everywhere in the NSSA region. Except for the semi-arid and

290 arid regions, most areas in the NSSA region show an albedo decrease when burned.

291 It's now clear that fires during the main burning season reduce the albedo of savan-

292 nas, woody savannas, crop/natural vegetation and grasslands as described above and shown

293   in figure 4b. The relatively few fires during the northern hemisphere summer months cause

294   an increase in albedo that is sufficiently large to dominate the annual average of the albedo

295   perturbation for all fire events shown in figure 4a. However, we note that the uncertainties

296   in both the albedo and the albedo perturbation reported in tables 3 and 4 during the summer

297   months for these land surface types are larger than the uncertainties for the winter months.

298   Thus, we conclude that the albedo reduction during the main fire season for these land sur-

299   face types is the more robust result. Higher spatio-temporal variability in the albedo during

300   the summer months accounts for greater uncertainty in characterizing the undisturbed al-

301   bedo during these months. Quantifying the albedo perturbation during these months is fur-

302   ther hampered by the relatively few fire events.

303   Figure 5 illustrates further the importance of albedo change in the fire months

304   (October – February). While albedo change in July is high (Fig. 5a), probably caused by

305   uncertainties of rapidly changing albedo that is correlated with the peak growing season,

306   the contribution is negligible when the monthly albedo changes are weighted by the frac-

307   tional fire count in each month (Fig. 5b). The albedo perturbations during the fire months

308   (Oct-Feb) stand out more prominently. Therefore, the albedo increase shown in Fig 4a is

309   due to uncertainties associated with other disturbances, while fires reduce or darken the sur-

310   face albedo as observed during the fire season (Fig. 4b). Additionally, the albedo decrease

311   after fires in February and December is associated with peak burning period of certain land

312   cover types depicted in Fig 3a (e.g. savannas, woody savannas, and croplands), probably

313   related to post-fire albedo darkening due to dissipation of charcoal and ash, or vegetation

314   growth. While the albedo increase after fires in January, October, and November is associ-

315   ated with peak burning period of other land cover types depicted in Fig 3b (e.g. grasslands,

316   shrublands and barren), probably related to the reduced vegetation moisture content in the

317   fall and winter, and resultant increasing combustion completeness during burning that leads

318   to more exposure of the underlying soils with higher albedo. This is consistent with the

319   findings of Hoffa et al. (1999) deduced from experimental burning, where decreasing vege-

320   tation moisture content and increasing fire line intensity were noted as the dry season pro-

321   gressed. Full details of albedo change by month and land cover types are given in Table 4.

322   The magnitude of albedo perturbations seen here (relative differences: -7% to 6 %) is con-

323   sistent with results from other studies (e.g. Govaerts et al. 2002) over the fire affected areas

324   in the NSSA region (5°N–10°N), where relative differences were found to range between -

325   8% and -5%. Our values are several factors smaller (<10) compared to points or tower

326   measurements immediately following a fire. For example, Scholes and Walker (1993) re-

327   ported a halving of African savanna albedo with a recovery to pre-fire values after 6 weeks.

328   These differences are to be expected given that MODIS albedo values are based on a 16-

329   day period and the pixel sizes are much larger (1 km).

330   *3.2   Post-fire albedo recovery*

331   There are many studies that have demonstrated the use of vegetation indices (e.g.

332   Normalized Difference Vegetation Index) and land cover characteristics (e.g land surface

333   temperature and albedo) as a measure of post-fire recovery, and which are described in a

334   review paper by Gita et al., (2012). In this study, we used post-fire surface changes to de-

335   scribe post-fire recovery in different ecosystems. This is deduced from the time it takes al-

336   bedo to return to within 5% of its pre-fire value. Our approach involves tracking albedo at

337   the pixel level comparing both burned and unburned (control or reference) pixel for the

338   same ecosystem. The unburned case was carefully selected from neighbouring pixels and

339   same land cover type that show similar albedo characteristics over an extended period of

340   time (at least two years), under similar conditions. The selection of a control can be tricky

341   and hampered by factors such as phenological effects, but the merits of a pixel-based ap-

342   proach outweigh its demerits (Gita et al., 2012; Lhermite et al., 2010; Veraverbeke et al.,

343   2010). Figure 6a shows a plot of albedo time series of both burned and unburned savannas

344   pixels, before and after fires for a period of about 3 years. Note that the interval between

345   data points is eight days. Figure 6b shows the same data, but zooming into the fire period in

346   order to show details of the albedo recovery after the fires. The pre-fire albedo values ex-

347   hibit a seasonal trend consistent with the vegetation phenology changes from senescence to

348   greenup, before and after the northern hemisphere winter in October–February. The corres-

349   ponding post-fire albedo values follow a similar trend, but have consistently lower values

350   after the fire is detected (gray-shaded region in Fig. 6a&b). Since the points represent al-

351   bedo every eight days, the recovery period in this case takes 288 days or about a year. We

352   used this approach to determine how long it took a burnt pixel to return to the pre-fire al-

353   bedo levels compared to a control pixel, which mimicked how the burnt pixel would have

354   behaved over several years without fires.

355   Figure 7 and Table 5 show post-fire albedo recovery of different land cover types in

356   northern sub-Saharan Africa for burn events that took place in 2003 tracked cumulatively at

357   3-month intervals over a period of seven years. At each step, we normalized by the total

358   number of tracked pixels in each land cover type. The albedo recovery after the first year

359   for some biomes such as croplands, closed broadleaf forests, deciduous broad leaf forests

360   and barren or sparse vegetation experienced a relatively rapid albedo recovery. Others such

361   as grassland, savannas, and woody savannas took a slower recovery path. Over 60% of the

362   burnt pixels for all the biomes recover their albedo to pre-fire period after the first year. By

363   the end of the second year after fires, over 80% of the burnt pixels recover their albedo to

364   pre-fire period, with some biomes such as deciduous broadleaf and closed shrublands

365   showing 100% albedo recovery. For the savannas and woody savannas, where 86% of

366   burning takes place, the recovery of the burnt pixels exceeds 97% after five years, and over

367   97% of the evergreen broadleaf forests burnt pixels recover after six years. The albedo re-

368   covery can be described by a simple exponential function:

369    $$R_t^c = ae^{-1/t^2} \qquad\qquad (3)$$

370   where, R_t^c is the % albedo recovery after t years for any land cover type c, and 'a' is

371   a contant (~50). This simple model fits well the observed albedo recovery for certain land

372   cover types (savanna, woody savanna, cropland, cropland or natural vegetation, and open

373   shrublands), where the model predicts a minimum albedo recovery of about 50% within the

374   first three months after fire. But it overestimates the albedo recovery of the other land cover

375   types (barren, evergreen broad leaf, closed shrublands, permanent wetlands, and deciduous

376   broadleaf) by about 30% within the first three months after the fire.

377   **4.   Conclusions**

378   We estimated the change of surface albedo due to fires over different land cover

379   types in the Northern Sub-Saharan Africa using data from the Moderate Resolution Imag-

380   ing Spectroradiometer (MODIS) from 2003–2011. We determined a decrease in albedo

381   over most land cover types due to fires (e.g. woody savannas (-0.00352 ± 0.00003) and sa-

382   vannas (-0.0.00391±0.00003), which accounted for >86% of the total MODIS fire count

383   between 2003 and 2011. Grasslands had a larger reduction (-0.00454± 0.00003) than the

384   savannas, but accounted for only about 5% of the total fire count. A few other land cover

385   types (e.g. Deciduous broad leaf: 0.00062 ± 0.00015 and barren: 0.00027 ± 0.00019)

386   showed an increase in albedo after fires, but accounted for less than 1% of the total fires.

387   The observed monthly albedo perturbation in each month for various biomes in NSSA is

388   variable, while the largest values observed in July, probably caused by uncertainties due to

389   rapidly changing albedo and correlated with the peak growing season. During the fire

390   season the albedo decrease is correlated with peak fire count of some land cover types (e.g.

391   savannas), possibly related to post-fire albedo darkening due to dissipation of charcoal and

392   ash, or vegetation regrowth. However, for certain land cover types (e.g. grasslands), there

393   there is albedo increase that is correlated with peak fire count, probably related to the re-

394   duced vegetation moisture content in the fall and winter, and the resultant increasing com-

395   bustion completeness during burning that leads to more exposure of the underlying soils

396   with higher albedo. The albedo recovery after fires progresses rapidly in year one, with the

397   savannas leading in recovery rate (>77%), and the deciduous broadleaf, permanent wet-

398   lands and barren showing the least recovery (56%). The persistence of surface albedo dark-

399   ening (or brightening, where applicable) is limited to about six to seven years, where at

400   least 98% of the burnt pixels recover to their pre-fire albedo for all land cover types. The

401   albedo recovery after fires can be described by a simple exponential function, regardless of

402   vegetation type.

403   The results summarized above provide a basis for assessing the sensitivity of the

404   Sub-Saharan Africa climate system to changes in surface albedo. It is clear that plausible

405   changes in surface albedo caused by wildfires vary in both space and time, depending on

406   the original vegetation type, which is dominated by the savannas.

414   **References**

415   Amiro B. D, Orchansky, A., Barr. A, Black, T., Chambers, S., Chapin, F., Goulden, M.,

416   Litvak, M., Liu, H., McCaughey, J., McMillan, A., & Randerson, J. (2006). The effect

417   of post-fire stand age on the boreal forest energy balance. Agricultural and Forest Me-

418   teorology, 140,41–50.

419   Amiro, B. D., MacPherson, J. I. & Desjardins, R. L. (1999). BOREAS flight measurements

420   of forest-fire effects on carbon dioxide and energy fluxes, Agric. For. Meteorol., 96,

421   199–208.

422   Andersen A. N., Cook G. D. & Williams R. J. (2003). Fire in Tropical Savannas: The Ka-

423   palga Experiment. Springer-Verlag, New York.

424   Andrea, M. O. & Merlet, P. (2001). Emission of trace gases and aerosols from biomass

425   burning. *Global Biogeochemical Cycles*, 15, 955–966.

426   Bremer, H., Kar, J., Drummond, J. R., Nichitu, F., Zou, J., Liu, J., Gille, J. C., et al. (2004).

427   Spatial and temporal variation of MOPITT CO in Africa and South America: A com-

428   parison with SHADOZ ozone and MODIS aerosol. *Journal of Geophysical Research*,

429   109 (D12304). doi:10.1029/2003JD004234.

430   Bosch, J. M., & Hewlett, J. D. (1982). A review of catchment experiments to determine the

431   effect of vegetation changes on water yield and evapotranspiration. *Journal of Hydrol-

432   ogy,* 55, 3–23.

433   Chambers, S. D., Beringer, J., Randerson, J. T., & Chapin, F. S., III (2005). Fire effects on

434   net radiation and energy portioning: contrasting responses of tundra and boreal forest

435   ecosystems.   *Journal   of   Geophysical   Research*,   110   (D09106).

436   doi:10.1029/2004JD005299.

437   Chapin, F. S., III, McGuire, A. D., Randerson, J., Pielke, R., Sr., Baldocchi, D., Hobbie, S.

438   E., Roulet, N., Eugster, W., Kasischke, W., Rastetter, E. B., Zimov, S. A., & Running,

439   S. W. (2000). Arctic and boreal ecosystems of western North America as components

440   of the climate system, Global Change Biol., 6, 211–223

441   Crutzen, P. J., & Andreae, M. O. (1990). Biomass burning in the tropics: Impacts on at-

442   mospheric chemistry and biogeochemical cycles. *Science*, 250, 1669–1778.

443   Dale, V. H., Joyce, L. A., Mcnulty, S., Neilson, R. P., Ayres, M. P., Flannigan, M. D., et al.

444   (2001). Climate Change and Forest Disturbances. *BioScience,* 51(9), 723–734.

445   Eva, H., & Lambin, E. F. (1998). Remote sensing of biomass burning in tropical regions:

446   sampling issues and multisensor approach. *Remote Sensing of Environment*, 64, 292–

447   315.

448   Farley, K. A., Jobbágy, E. G., & Jackson, R. B. (2005). Effects of afforestation on water

449   yield: a global synthesis with implications for policy. *Global Change Biology*, 11,

450   1565–1576.

451   Friedl, M. A., Sulla-Menashe, D., Tan, B., Schneider, A., Ramankutty, N., Sibley, A., &

452   Huang., X. (2010), MODIS Collection 5 global land cover: Algorithm refinements and

453   characterization of new datasets. *Remote Sens. Environ.*, 114, 168–182,

454   doi:10.1016/j.rse.2009.08.016.

455   Fuller, O. D., & Ottke, C. (2002). Land cover, rainfall and land-surface albedo in West

456   Africa. *Climatic Change,* 54, 181–204.

457   Gao, F., Morisette, J. T., Wolfe, R. E., Ederer, G., Pedelty, J., Masuoka, E., Myneni, R.,

458   Tan, B., & Nightingale, J. (2008). An Algorithm to produce temporally and spatially

459   continuous MODIS-LAI time series. *IEEE Geoscience and Remote sensing Letters*, 5

460   (1), 60–64.

461   Gatebe, C. K., King, M. D., Platnick, S., Arnold, G. T., Vermote, E. F., & Schmid, B.

462   (2003). Airborne spectral measurements of surface-atmosphere anisotropy for several

463   surfaces and ecosystems over southern Africa. *Journal of Geophysical Research*, 108,

464   8489. doi:10.1029/2002JD002397.

465   Giglio, L., Descloitres, J., Justice, C. O., & Kaufman, Y. (2003). An enhanced contextual

466   fire detection algorithm for MODIS. *Remote Sensing of Environment*, 87, 273–282.

467   Gitas, I., Mitri, G., Veraverbeke, S., and Polychronaki. A. (2012). Advances in Remote

468   Sensing of Post-Fire Vegetation Recovery Monitoring - A Review, Remote Sensing of

469   Biomass - Principles and Applications, L. Fatoyinbo (Ed.), ISBN: 978-953-51-0313-4,

470   InTech, DOI: 10.5772/20571: http://www.intechopen.com/books/remote-sensing-of-

471   biomass-principles-and-applications/advances-in-remote-sensing-of-post-fire-

472   monitoring-a-review.

473   Govaerts, Y. M., Pereira, J. M., Pinty, B., & Mota, B. (2002). Impact of fires on surface

474   albedo dynamics over the African continent. *Journal of Geophysical Research*, 107

475   (D22, 4629), doi:10.1029/2002JD002388.

476   Hoffa, E. A., Ward, D. E., Hao, W. M., Susott, R. A., & Wakimoto, R. H. (1999). Season-

477   ality of carbon emissions from biomass burning in a Zambian savanna. *Journal of

478   Geophysical Research*, 104(D11), 13841–13853.

479   Ichoku, C., Giglio, L., Wooster, M. J., & Remer, L. A. (2008). Global characterization of

480   biomass-burning patterns using satellite measurements of radiative energy, *Remote

481   Sensing of Environment*, 112, 2950–2962.

482   Jackson, R. B., Jobbágy, E. G., Avissar, R., Roy, S. B., Barrett, D. J., Cook, C. W., et al.

483   (2005). Trading water for carbon with biological sequestration. *Science*, 310, 1944–

484   1947.

485   Jin, Y., & Roy, D. P. (2005). Fire-induced albedo change and its radiative forcing at the
486   surface in northern Australia. *Geophysical Research Letters*, 32, L13401. doi:10.1029/
487   2005GL022822.

488   Justice, C. O., Giglio, L., Korontzi, S., Owens, J., Morisette, J., Roy, D., Descloitres, J., Al-
489   leaume, S., Petitcolin, F., & Kaufman, Y. (2002). The MODIS fire products, *Remote
490   Sensing of Environment*, 83, 244–262.

491   Le Houérou, H. N. (1996). Climate change, drought and desertification: review. *Journal of
492   Arid Environments*, 34, 133–185.

493   Lhermitte, S., Verbesselt, J., Verstraeten, W.W., Coppin, P., (2010). A pixel based regen-
494   eration index using time series similarity and spatial context. Photogrammetric Engi-
495   neering & Remote Sensing 76 (6), 673–682.

496   King, M. D., Strange, M. G., Leone, P., & Blaine, L. R. (1986). Multiwavelength scanning
497   radiometer for airborne measurements of scattered radiation within clouds. J*ournal of
498   Atmospheric and Oceanic Technology*, 3, 513–522.

499   O'Hallon, T. L., Law, B. E., Goulden, M. L., Wang. Z., Barr, J. G., Schaaf, C., Brown, M.,
500   Fuentes, J. D., Gockede, M., Black, A. & Engel, V. (2012). Radiative forcing of natu-
501   ral forest disturbance, Global Change Biology, 18, 555–565, doi: 10.1111/j.1365-
502   2486.2011.02577.x

503   Levia, D. F., & Frost, E. E. (2003). A review and evaluation of stemflow literature in the
504   hydrologic and biogeochemical cycles of forested and agricultural ecosystems. *Journal
505   of Hydrology*, 274, 1–29.

506   Randerson J. T, Liu, H, Flanner, M.G. et al. (2006). The impact of boreal forest fire on cli-
507   mate warming. Science, 314, 1130–1132. DOI: 10.1126/science.1132075.

508 Roberts, G., M. J. Wooster, and E. Lagoudakis (2009). Annual and diurnal African biomass
509   burning temporal dynamics, *Biogeosciences*, 6, 849–866.

510 Román, M. O., Gatebe, C. K., Schaaf, C., Poudyal, R., Wang, Z., & King, M. D. (2011).
511   Variability in surface BRDF at different spatial scales (30 m–500 m) over a mixed
512   agricultural landscape as retrieved from airborne and satellite spectral measurements.
513   *Remote Sensing of Environment*, 115, 2184-2203. doi:10.1016/j.rse.2011.04.012.

514 Román, M. O., Schaaf, C. B., Lewis, P., Gao, F., Anderson, G. P., Privette, J. L., Strahler,
515   A. H., Woodcock, C. E., Barnsley, M. (2010). Assessing the coupling between surface
516   albedo derived from MODIS and the fraction of diffuse skylight over spatially-
517   characterized landscapes. Remote Sensing of Environment, 114, 738–760.

518 Roy, D. P., Boschetti, L., Justice, C. O., & Ju, J. (2008). The Collection 5 MODIS Burned
519   Area Product - Global Evaluation by Comparison with the MODIS Active Fire Pro-
520   duct. *Remote Sensing of Environment*, 112, 3690–3707.

521 Salomon, J., Schaaf, C. B., Strahler, A. H., Gao, F., Jin, Y. (2006). Validation of the
522   MODIS bidirectional reflectance distribution function and albedo retrievals using
523   combined observations from the Aqua and Terra Platforms, IEEE Transactions of.
524   Geoscience and Remote Sensing, 44 (6), 1555–1565.

525 Schaaf, C. B., Gao, F., Strahler, A. H., Lucht, W., Li, X., Tsang, T., Strugnell, N. C., et al.
526   (2002). First operational BRDF, albedo and aadir reflectance products from MODIS.
527   *Remote Sensing of Environment*, 83, 135–148.

528 Sheuyange, A., Oba, G., & Weladji, R. B. (2005). Effects of anthropogenic fire history on
529   savanna vegetation in northeastern Namibia. *Journal of Environmental Management*,
530   75, 189–198.

531 Scholes, R. J., & Archer, S. R. (1997). Tree–grass interactions in savannas. *Annual Review*

532   *of Ecological Systems*, 28, 517–544.

533   Scholes, R. J., & Walker, B. H. (1993). An African savanna synthesis of the Nylsvley

534   study, Cambridge University Press, Campbridge, 306p.

535   Veraverbeke, S., Lhermitte, S., Verstraeten, W. W., & Goossens, R. (2010). The temporal

536   dimension of differenced Normalized Burn Ratio (dNBR) fire/burn severity studies:

537   the case of the large 2007 Peloponnese wildfires in Greece. Remote Sensing of Envi-

538   ronment 114: 2548-2563.

539   Wanner, W., Strahler, A. H., Hu, B., Lewis, P., Muller, J.-P., Li, X., Schaaf, C. L. B. &

540   Barnsley, M. J. (1997). Global retrieval of bidirectional reflectance and albedo over

541   land from EOS MODIS and MISR data: Theory and algorithm. *Journal of Geophysi-*

542   *cal Res*earch, 102, 17143–17162.

543   Zhang, L, Dawes, W. R., & Walker, G. R. (2001). Response of mean annual evapotranspi-

544   ration to vegetation changes at catchment scale. *Water Resources Research*, 37, 701–

545   708.

546

547

547   Table 1: Average gap-filling error in albedo for different land cover types in the NSSA

MODIS Tile: h-20,v-07	N= 600 pixels; Error (%)			
	1-gap	2-gaps	3-gaps	4-gaps
Barren/ sparsely veg.	-0.15	0.02	1.32	0.02
Savannas	-1.73	-2.92	-7.32	-15.5
Woody Savannas	-1.93	-5.53	-12.9	-21.13
Grassland	-0.47	-1.22	-1.45	-1.7
Open shrubland	-0.02	0.82	1.37	-0.43
Crop/nat. vegetation	-1.45	-3.6	-8.93	-13.71
Closed shrub	-1.26	-1.28	0.12	-9.44
Cropland	-0.98	-0.45	-5.79	-10.94
Deciduous broadleaf	-2.9	-5.25	-12.19	-17.41

548

548   Table 2: Accuracy and uncertainty values resulting from a 32-day comparison between airborne (CAR) and satellite-derived

549   (MODIS) albedos using two different gap-filling approaches.

a. All Days	10°≤ SZA ≤45° (n=289)			45°≤ SZA ≤75° (n=193)		
DOY 159–190	Aircraft/(CAR)	MODIS/albedo1	MODIS/albedo2	Aircraft/(CAR)	MODIS/albedo1	MODIS/albedo2
Accuracy	0.0042	-0.0286	-0.0333	-0.0096	-0.0495	-0.0570
Uncertainty	0.0082	0.0296	0.0341	0.0184	0.0526	0.0589

550

551

551   Table 3: Albedo of unburnt pixel from MODIS (2003-2011) for different land cover types in the NSSA

Landcover	Jan	Feb	Mar	April	May	June	July	Aug	Sept	Oct	Nov	Dec
Barren/ sparsely veg.	0.169± 0.032	0.187± 0.028	0.196± 0.004	0.168± 0.039	0.176± 0.034	0.187± 0.040	0.208± 0.027	0.187± 0.028	0.174± 0.034	0.212± 0.033	0.201± 0.036	0.191± 0.075
Savannas	0.135± 0.004	0.147± 0.002	0.159± 0.002	0.160± 0.005	0.162± 0.005	0.158± 0.005	0.151± 0.013	0.143± 0.019	0.135± 0.014	0.147± 0.003	0.130± 0.003	0.130± 0.002
Woody Sa- vannas	0.128± 0.004	0.137± 0.002	0.148± 0.003	0.151± 0.005	0.155± 0.005	0.157± 0.007	0.145± 0.014	0.147± 0.019	0.137± 0.009	0.144± 0.002	0.130± 0.002	0.126± 0.003
Evergreen broadleaf	0.123± 0.003	0.127± 0.002	0.140± 0.006	0.140± 0.005	0.138± 0.005	0.148± 0.008	0.140± 0.014	0.138± 0.009	0.140± 0.017	0.130± 0.014	0.130± 0.007	0.120± 0.006
Grassland	0.155± 0.007	0.165± 0.004	0.175± 0.004	0.180± 0.006	0.187± 0.012	0.189± 0.012	0.166± 0.015	0.158± 0.012	0.155± 0.017	0.161± 0.006	0.145± 0.003	0.151± 0.004
Open shru- bland	0.167± 0.006	0.184± 0.006	0.195± 0.015	0.193± 0.011	0.201± 0.004	0.209± 0.016	0.219± 0.032	0.228± 0.054	0.183± 0.022	0.164± 0.009	0.155± 0.008	0.164± 0.007
Crop/nat. vegetation	0.155± 0.003	0.162± 0.003	0.171± 0.003	0.176± 0.007	0.178± 0.007	0.174± 0.006	0.157± 0.014	0.161± 0.017	0.152± 0.011	0.157± 0.003	0.151± 0.004	0.155± 0.003
Closed shrub	0.146± 0.004	0.153± 0.004	0.164± 0.004	0.161± 0.008	0.158± 0.009	0.158± 0.020	0.157± 0.015	0.136± 0.013	0.130± 0.012	0.149± 0.004	0.140± 0.003	0.143± 0.004
Cropland	0.155± 0.004	0.164± 0.006	0.170± 0.004	0.172± 0.004	0.167± 0.006	0.170± 0.015	0.157± 0.014	0.144± 0.017	0.146± 0.018	0.160± 0.008	0.148± 0.006	0.152± 0.004
Persistent wetland	0.117± 0.012	0.126± 0.006	0.137± 0.007	0.140± 0.006	0.141± 0.006	0.144± 0.016	0.142± 0.016	0.132± 0.028	0.114± 0.015	0.134± 0.010	0.122± 0.010	0.116± 0.008
Deciduous broadleaf	0.140± 0.004	0.145± 0.004	0.153± 0.005	0.153± 0.002	0.151± 0.013	0.147± 0.031	0.136± 0.012	0.114± 0.033	0.150± 0.024	0.146± 0.011	0.139± 0.003	0.139± 0.004

552

553

553   Table 4: Fire frequency and albedo change due fires from MODIS (2003-2011) for different land cover types in the NSSA

	Fire count (%)	Albedo Change (x 10^{-3})											
		Jan	Feb	Mar	Apr	May	Jun	Jul	Aug	Sep	Oct	Nov	Dec
Barren/ sparsely veg.	0.18	4.4± 9.0	-0.2± 7.5	0.3± 5.2	0.7± 10.7	-4.8± 13.0	-1.7± 19.4	0.7± 9.6	0.3± 4.4	0.7± 6.8	-1.8± 7.3	0.1± 14.1	-2.2± 5.4
Savannas	37.73	-2.0± 3.5	-3.9± 4.3	0.4± 5.0	1.0± 3.5	2.1± 3.5	3.2± 4.8	4.4± 8.1	-2.4± 9.8	-0.3± 6.0	4.5± 4.8	0.3± 2.6	-2.7± 3.4
Woody Savannas	48.69	-1.6± 3.7	-3.6± 4.0	-1.1± 3.4	-0.2± 2.5	-0.1± 2.5	2.5± 5.1	6.0± 15.0	-0.2± 10.4	1.0± 7.4	3.0± 3.7	0.3± 2.8	-1.6± 3.2
Evergreen broad-leaf	0.71	1.4± 3.4	-4.9± 7.2	0.5± 6.1	-1.0± 5.9	-3.5± 8.7	-4.0± 12.0	2.7± 18.9	2.0± 14.5	5.3± 16.0	-1.3± 15.0	-0.2± 4.9	-0.9± 4.3
Grassland	4.78	-0.5± 2.8	-3.2± 4.1	-0.5± 3.8	1.7± 3.9	-1.6± 3.7	3.1± 6.9	8.2± 14.3	4.5± 12.5	-2.3± 4.9	-1.1± 3.2	1.0± 3.4	-0.7± 3.7
Open shrubland	0.67	0.4± 3.1	-2.3± 3.8	-0.7± 4.5	1.2± 5.2	-1.3± 3.5	4.7± 7.1	7.3± 10.4	2.6± 12.3	-1.7± 6.3	-0.6± 2.6	1.1± 3.2	-1.3± 3.2
Crop/nat. vegeta-tion	5.59	-0.5± 2.4	-3.0± 3.0	0.5± 4.6	0.2± 3.0	-0.2± 4.0	4.2± 7.3	1.0± 14.1	3.4± 15.2	0.8± 6.5	-0.6± 1.6	0.7± 3.3	-0.4± 2.8
Closed shrub	0.16	0.9± 3.0	-3.8± 5.2	2.1± 3.6	3.0± 4.8	0.3± 7.4	0.4± 13.2	7.9± 15.8	0.9± 11.8	3.6± 7.6	4.0± 4.1	1.7± 2.3	-1.3± 4.3
Cropland	0.89	0.9± 3.8	-3.3± 3.7	0.9± 6.0	1.6± 4.5	-2.0± 5.2	1.3± 7.6	0.9± 13.0	3.2± 16.7	0.7± 6.0	-0.1± 3.3	0.5± 5.0	0.9± 2.3
Persistent wetland	0.34	4.1± 4.8	-3.4± 4.8	-0.4± 5.9	2.0± 4.9	-0.3± 10.0	-2.0± 7.1	4.6± 16.2	-1.8± 7.8	1.2± 7.8	0.9± 9.9	0.4± 5.8	1.4± 7.2
Deciduous broad-leaf	0.26	-0.9± 2.6	-3.3± 4.5	-1.0± 5.0	0.4± 5.3	2.7± 9.3	0.2± 5.3	2.4± 6.9	-0.4± 4.6	-0.2± 1.1	6.4± 10.7	0.0± 4.8	-1.6± 3.3
Total sum	100	6.7	-34.9	0.8	10.6	-8.7	11.9	46.0	12.1	8.7	13.1	5.9	-10.6

554

555

555   Table 5: Post-fire albedo recovery after every three months

|						No of burnt pixels with full-albedo recovery (%)					
Yrs	Savannas	Woody Savanas	Grasslands	Cropland	Barren	Cropland Nat. Veg	Evergreen-broad-leaf	Open Shrublands	Closed Shrublands	Permanent Wetlands	Deciduous broad-Leaf
0.25	49.25	41.18	34.47	24.58	22.07	45.94	25.46	35.92	24.93	23.47	20.92
0.49	55.47	44.61	43.71	49.49	31.06	53.61	33.72	43.69	33.99	33.60	30.09
0.74	60.94	53.06	51.35	62.63	43.05	62.12	45.87	54.13	45.61	45.87	42.69
0.99	77.93	81.77	73.02	71.38	55.59	79.79	58.26	64.32	56.66	56.53	55.87
1.23	83.71	88.01	76.87	77.10	61.58	82.39	64.91	69.17	62.61	63.73	62.18
1.48	84.13	88.21	77.45	79.12	64.31	83.17	67.20	71.60	65.16	66.93	65.04
1.73	84.64	88.49	78.91	82.32	68.66	84.15	70.87	75.49	69.69	70.93	69.91
1.97	87.99	91.99	88.73	85.35	73.02	88.17	75.92	79.61	74.22	76.27	74.50
2.22	92.00	94.17	90.25	87.21	76.57	91.10	78.90	82.52	78.75	79.20	77.94
2.47	92.18	94.21	90.47	87.88	77.11	91.16	79.59	83.01	79.32	79.47	78.51
2.71	92.31	94.33	90.91	89.56	79.29	91.62	81.42	84.71	81.30	81.60	80.80
2.96	93.21	95.49	94.11	91.58	85.01	94.28	84.40	87.62	84.99	85.07	84.53
3.21	95.75	96.83	94.98	93.43	87.74	95.19	86.70	89.81	87.82	87.73	87.39
3.45	95.88	96.90	95.56	94.44	89.37	95.52	88.07	91.26	89.52	89.60	89.11
3.70	95.93	96.99	95.78	95.45	91.28	95.78	89.91	92.96	91.50	91.47	91.40
3.95	96.20	97.31	97.16	96.46	93.19	96.56	91.51	94.42	93.48	93.33	93.41
4.19	97.71	98.26	97.96	97.14	94.55	97.21	93.35	95.15	94.90	94.40	94.84
4.44	97.76	98.30	98.11	97.31	95.37	97.40	94.04	95.87	95.47	95.20	95.70
4.68	97.83	98.34	98.11	97.98	96.46	97.60	94.95	96.84	96.60	96.27	96.85
4.93	98.06	98.55	98.55	98.15	97.00	98.05	95.18	97.09	96.88	96.53	97.13
5.18	99.35	99.30	99.20	98.65	98.09	98.64	96.10	98.06	98.02	97.60	97.99
5.42	99.39	99.32	99.27	98.99	98.37	98.64	96.33	98.30	98.30	97.87	98.28
5.67	99.41	99.36	99.27	98.99	98.37	98.64	96.33	98.30	98.30	97.87	98.28
5.92	99.50	99.47	99.71	99.16	98.91	98.77	96.79	99.03	98.87	98.40	98.85
6.16	99.87	99.90	99.93	99.66	99.73	99.48	97.71	99.76	99.72	99.20	99.71
6.41	99.88	99.91	100.00	99.83	100.00	99.55	97.94	100.00	100.00	99.47	100.00
6.66	99.88	99.91	100.00	100.00	100.00	99.94	97.94	100.00	100.00	99.47	100.00

556
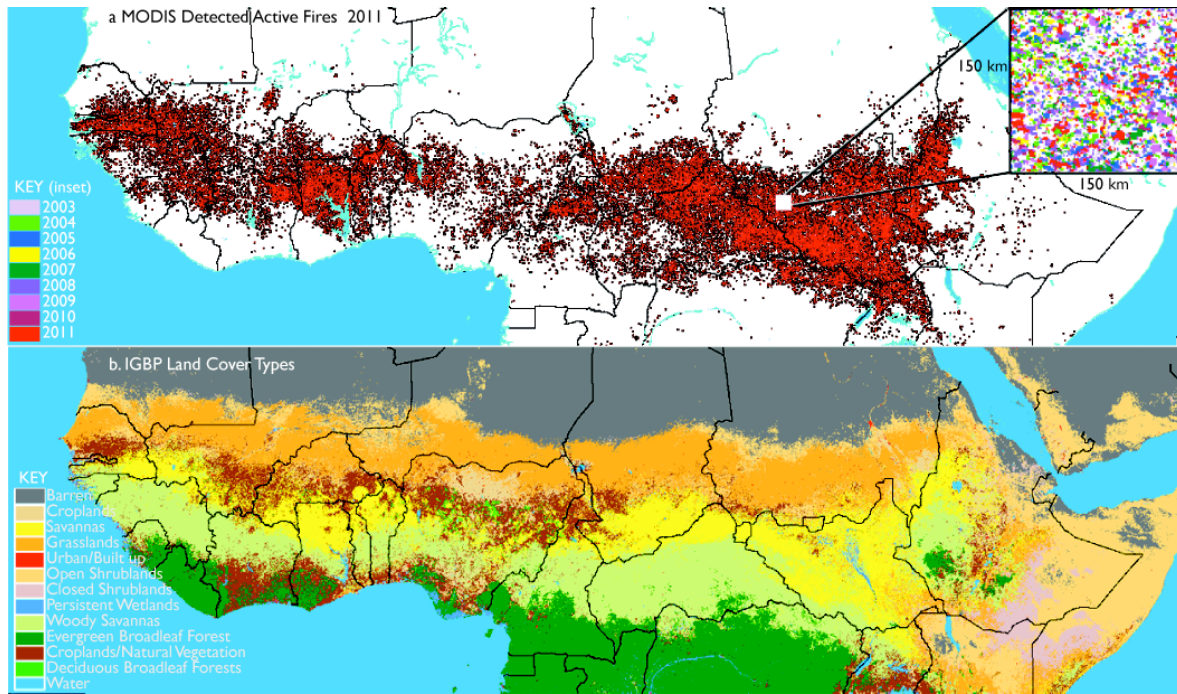
557
558   Fig. 1.   a. Spatial distribution of MODIS detected fires in 2011. A similar pattern
559   was observed for each year between 2003-2011. The inset shows fire dis-
560   tribution for all the years (2003-2011) over a small area, 150 km x 150 km
561   in Southern Sudan. Most fires occurred in the savannas and grasslands. b.
562   Spatial distribution of the main types of land cover in the Northern Sub-
563   saharan Africa. Barren or sparsely vegetated lands occupy the largest
564   area (25%), followed by woody savannas and grasslands, each at 15% (cf.
565   section 3.1).
566

567

567
568

569
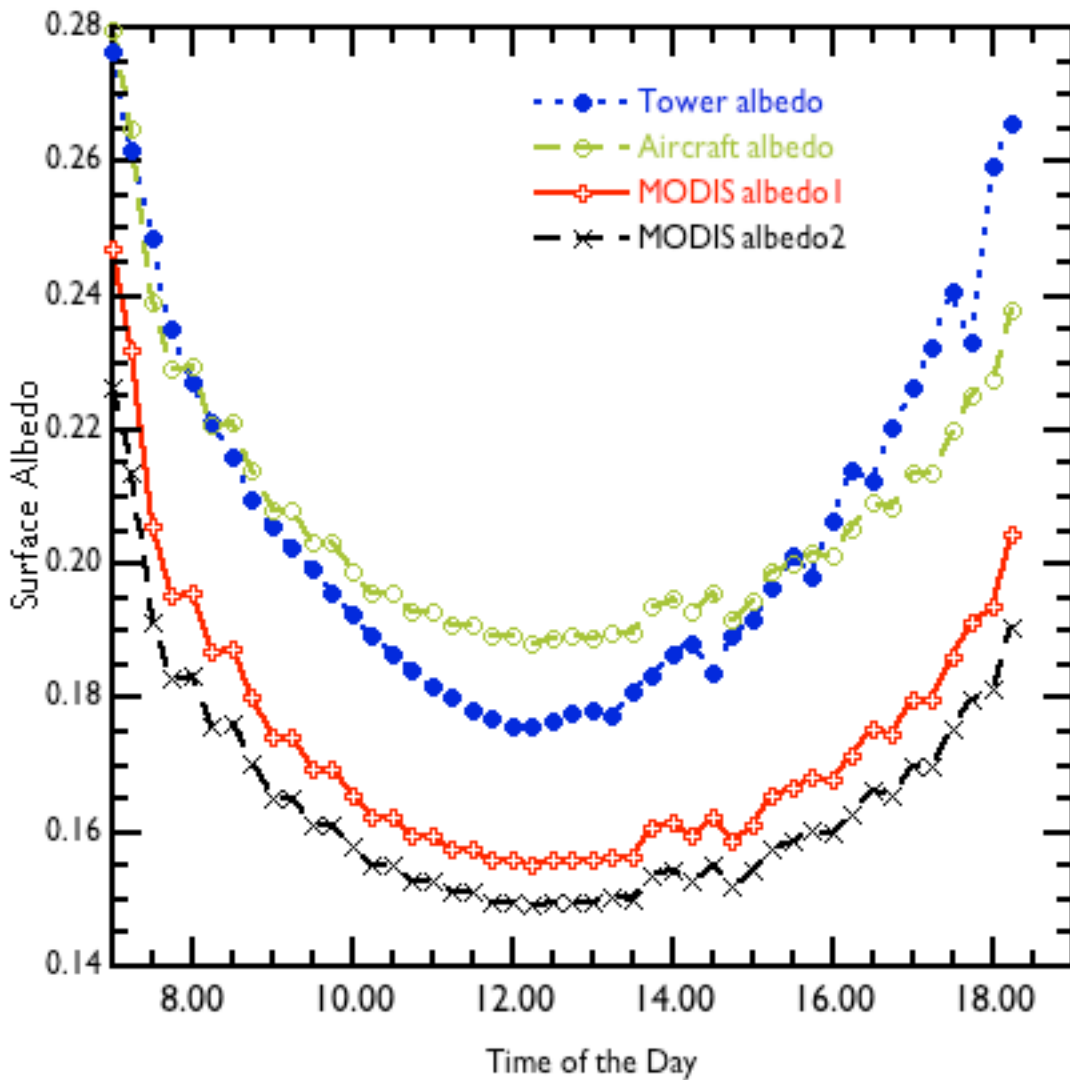
570   Fig. 2. Comparisons between instantaneous albedos (15-min intervals) derived from air-

571   borne CAR, tower-based measurements, and satellite MODIS using two different

572   gap filled approaches over the CART site on 24 June 2007 during CLASIC Field

573   Campaign. The difference between daily average MODIS and Aircraft/Tower al-
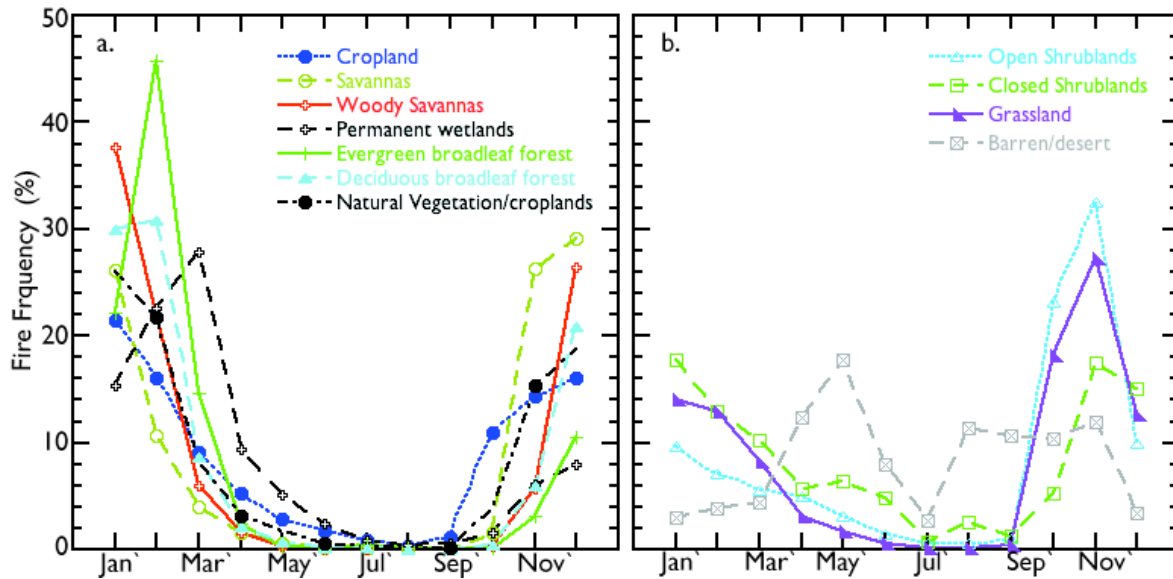
574   bedo varies from 15-20% (cf. Table 2).

575

575

576

577 Fig. 3. Monthly Fires detected by MODIS (2003–2011) normalized by the total fires for

578   each land cover type in Northern Sub-Saharan Africa. Most fires occur between

579   October and March with peak for some cover types around a. January, or, b.

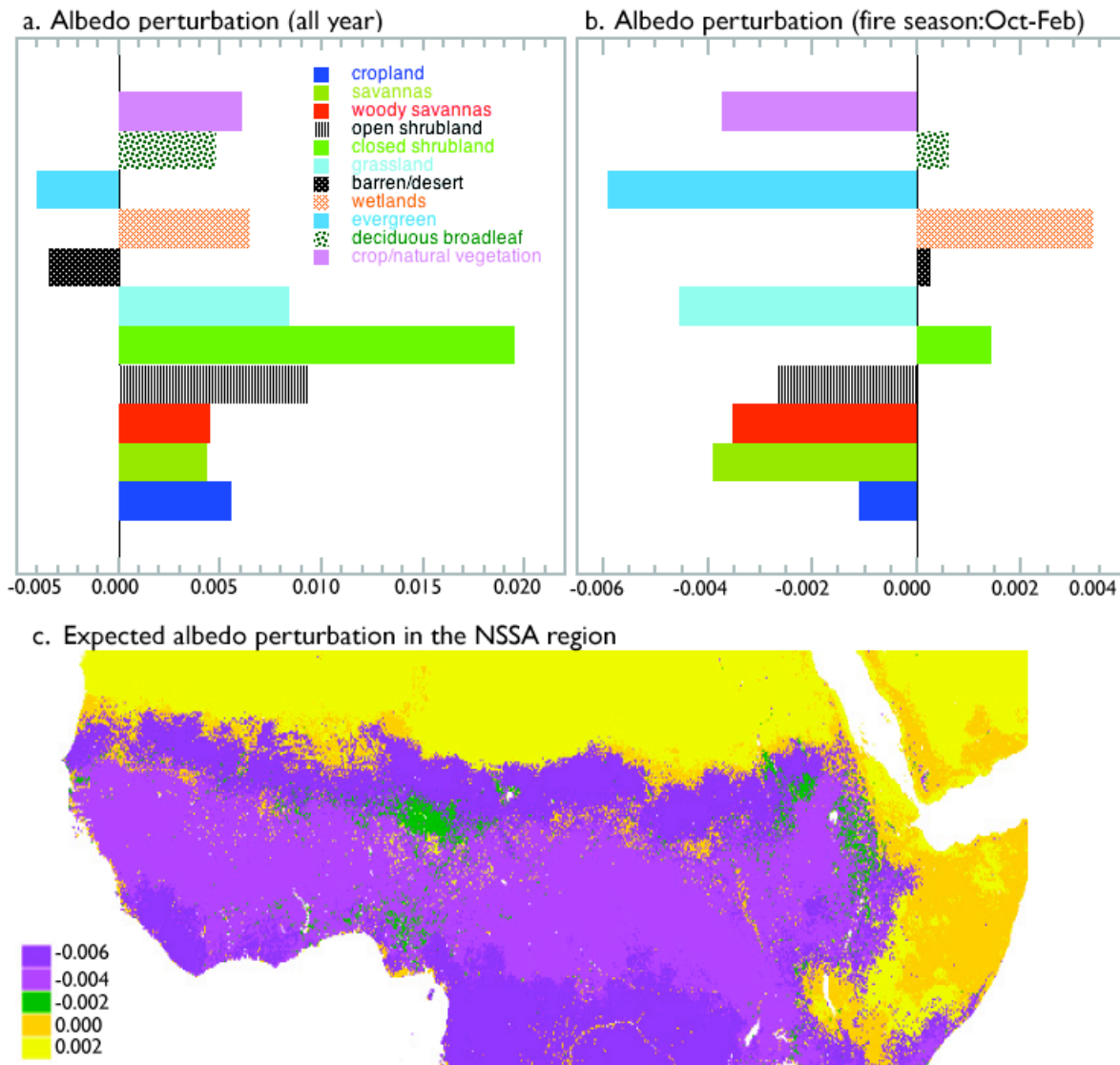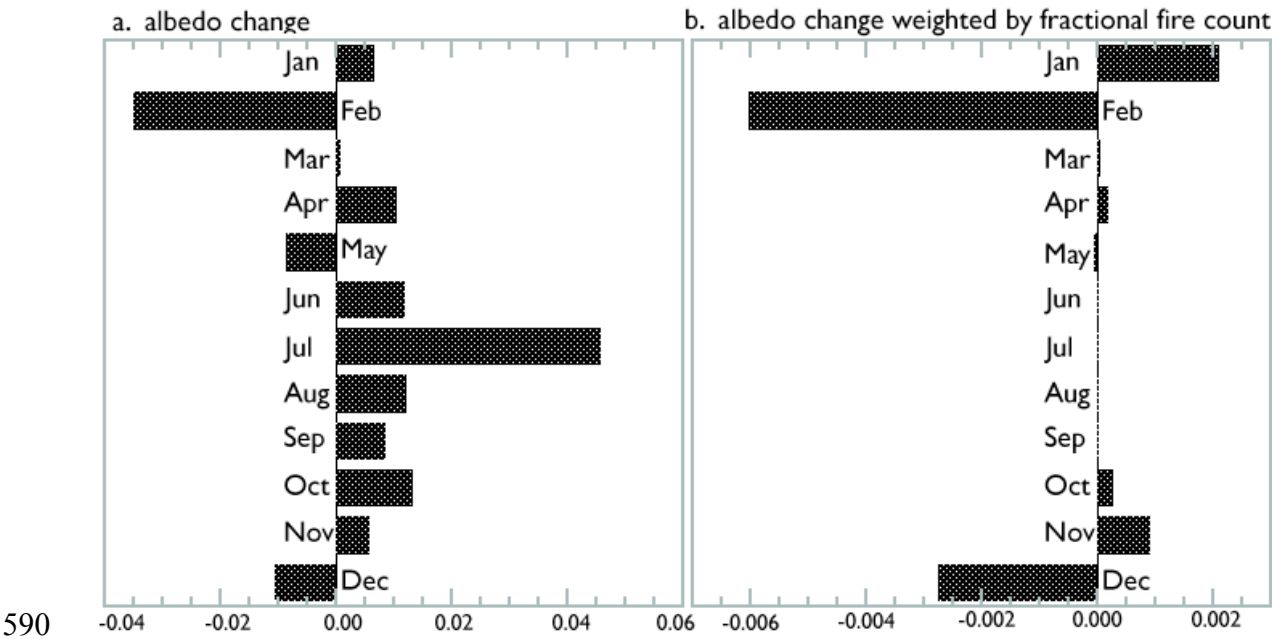580   November. Barren or desert land cover type has a peak around May.

581

582
583

583

Fig. 4.   a.- Albedo perturbation for different land cover types averaged over nine
          years (2003-2011). c. Albedo perturbation for the fire season only (Oct –
          Feb). c. shows albedo perturbation if fires would burn everywhere in the
          NSSA region.

588

589

589

590

591 Fig. 5. a. Monthly change in albedo associated with wildfires for all land cover
592   types combined. b. Same as in a., but weighted by fire count observed by
593   MODIS in each month and normalized by total fire count.
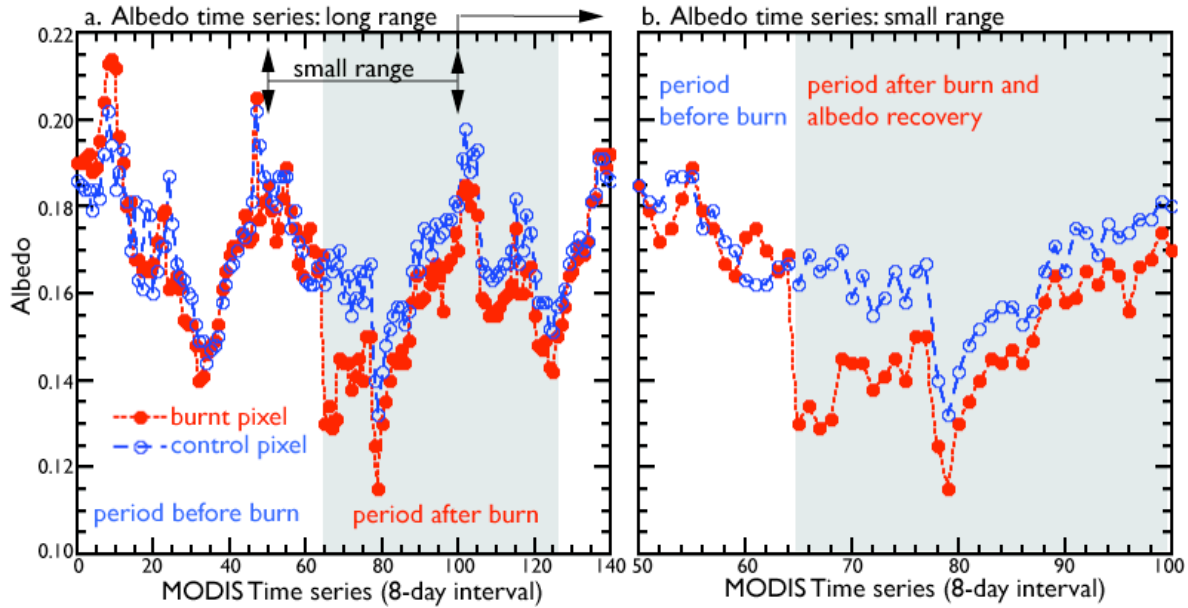594

594

595

596

597 Fig. 6.   a. An example of albedo time series of a burned savanna pixel (red line)
598   and its corresponding control pixel (blue line) beginning 10 Feb 2005 to 2
599   Feb 2008. The gray-shaded area represents mostly the post-fire period. b.
600   Same as a., but zooming into the post-fire period. The control pixel mim-
601   ics how the burned pixel would have behaved without fire. Fire was de-
602   tected on 26 June 2006 and its effect on albedo lasted for about 288 days.
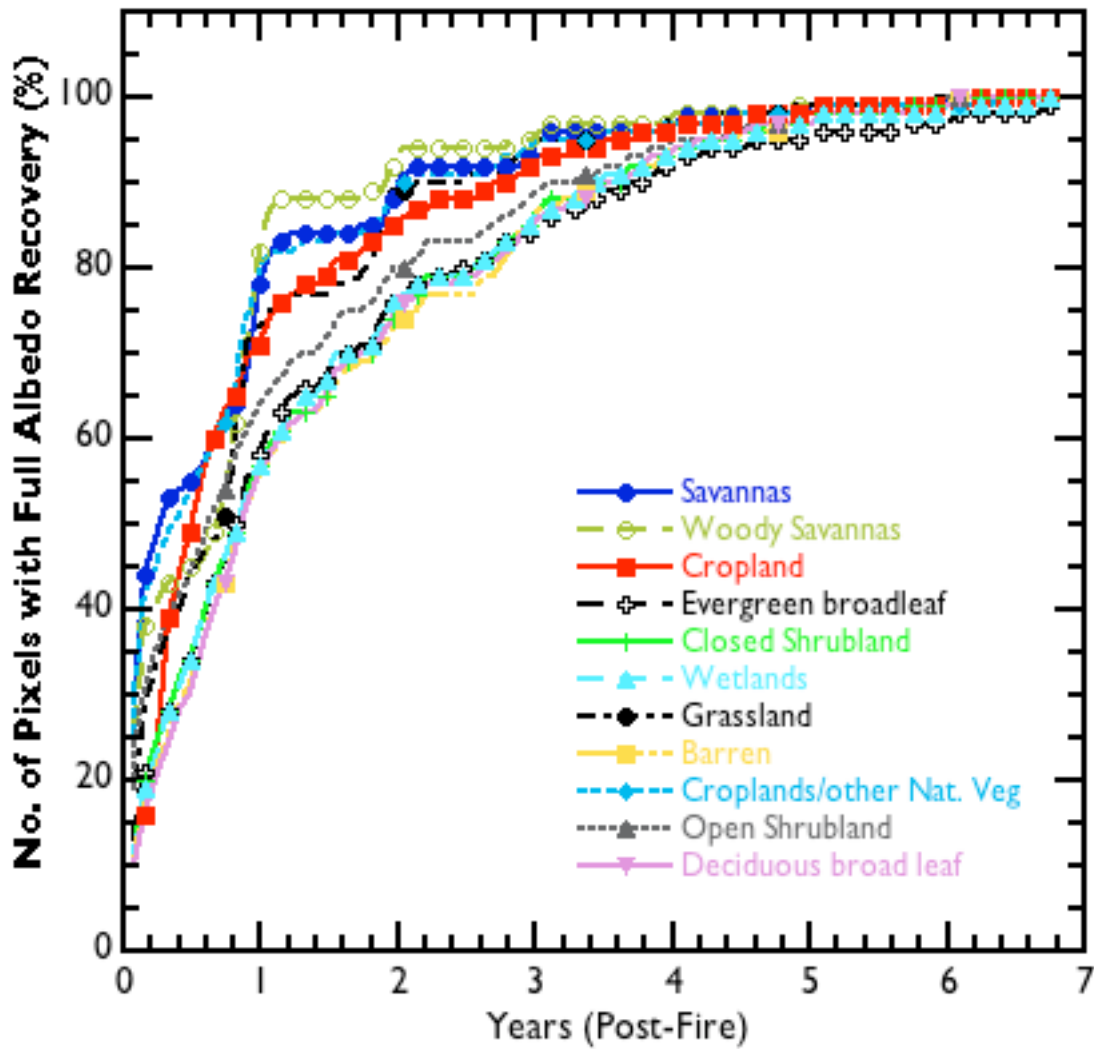
603

604

604

605

606 Fig. 7.   Percentage of pixels burned in 2003 that has recovered by each subse-
607   quent year tracked over a period of seven years for different land cover
608   types in northern sub-Saharan Africa. Points are plotted every 90 days.

609